Air Force Institute of Technology

AFIT Scholar

Faculty Publications

5-26-2011

Complementary Metal-oxide Semiconductor-compatible Detector Materials with Enhanced 1550 nm Responsivity via Sn-doping of Ge/Si(100)

Richard T. Beeler
Arizona State University

Jay Mathews
Arizona State University

Mee-Yi Ryu
Kangwon National University

Yung-Kee Yeo
Air Force Institute of Technology

Jose Menendez
Arizona State University

See next page for additional authors

Follow this and additional works at: https://scholar.afit.edu/facpub

Part of the Physics Commons, and the Semiconductor and Optical Materials Commons

Recommended Citation

Radek Roucka, Richard Beeler, Jay Mathews, Mee-Yi Ryu, Yung Kee Yeo, José Menéndez, John Kouvetakis; Complementary metal-oxide semiconductor-compatible detector materials with enhanced 1550 nm responsivity via Sn-doping of Ge/Si(100). Journal of Applied Physics 15 May 2011; 109 (10): 103115. https://doi.org/10.1063/1.3592965

This Article is brought to you for free and open access by AFIT Scholar. It has been accepted for inclusion in Faculty Publications by an authorized administrator of AFIT Scholar. For more information, please contact richard.mansfield@afit.edu.

Authors
Richard T. Beeler, Jay Mathews, Mee-Yi Ryu, Yung-Kee Yeo, Jose Menendez, and John Kouvetakis

This article is available at AFIT Scholar: https://scholar.afit.edu/facpub/1247

Journal of Applied Physics

RESEARCH ARTICLE | MAY 26 2011

Complementary metal-oxide semiconductor-compatible detector materials with enhanced 1550 nm responsivity via Sn-doping of Ge/Si(100)

Radek Roucka; Richard Beeler; Jay Mathews; Mee-Yi Ryu; Yung Kee Yeo; José Menéndez; John Kouvetakis

Journal of Applied Physics 109, 103115 (2011)
https://doi.org/10.1063/1.3592965

View Online

Export Citation

CrossMark

Downloaded from http://pubs.aip.org/aip/jap/article-pdf/doi/10.1063/1.3592965/15075199/103115_1_online.pdf

AIP Advances
Why Publish With Us?
25 DAYS average time to 1st decision
740+ DOWNLOADS average per article
INCLUSIVE scope
Learn More
AIP Publishing

Complementary metal-oxide semiconductor-compatible detector materials with enhanced 1550 nm responsivity via Sn-doping of Ge/Si(100)

Radek Roucka,[1,a)] Richard Beeler,[1] Jay Mathews,[2] Mee-Yi Ryu,[3] Yung Kee Yeo,[4] José Menéndez,[2] and John Kouvetakis[1]
[1]*Department of Chemistry and Biochemistry, Arizona State University, Tempe, Arizona 85287-1604, USA*
[2]*Department of Physics, Arizona State University, Tempe, Arizona 85287-1504, USA*
[3]*Department of Physics, Kangwon National University, Chuncheon, Kangwon-Do 200-701, Korea*
[4]*Department of Engineering Physics, Air Force Institute of Technology, Wright Patterson AFB, Ohio 45433, USA*

(Received 17 February 2011; accepted 22 April 2011; published online 26 May 2011)

Previously developed methods used to grow $Ge_{1-y}Sn_y$ alloys on Si are extended to Sn concentrations in the $10^{19}-10^{20}$ cm^{-3} range. These concentrations are shown to be sufficient to engineer large increases in the responsivity of detectors operating at 1550 nm. The dopant levels of Sn are incorporated at temperatures in the 370–390 °C range, yielding atomically smooth layers devoid of threading defects at high growth rates of 15–30 nm/min. These conditions are far more compatible with complementary metal-oxide semiconductor processing than the high growth and processing temperatures required to achieve the same responsivity via tensile strain in pure Ge on Si. A detailed study of a detector based on a Sn-doped Ge layer with 0.25% (1.1×10^{20} cm^{-3}) Sn range demonstrates the responsivity enhancement and shows much better *I-V* characteristics than previously fabricated detectors based on $Ge_{1-y}Sn_y$ alloys with $y = 0.02$. © *2011 American Institute of Physics*. [doi:10.1063/1.3592965]

Downloaded from http://pubs.aip.org/aip/jap/article-pdf/doi/10.1063/1.3592965/15075199/103115_1_online.pdf

I. INTRODUCTION

Alloys of Ge and Sn are attracting increasing attention as the only group-IV system with a predicted direct bandgap and enhanced absorption in the near-infrared. While different synthetic approaches have been pursued,[1–8] the chemical vapor deposition (CVD) method introduced by Bauer and co-workers,[10] which uses mixtures of digermane (Ge_2H_6) and deuterated stannane (SnD_4), is particularly attractive for its simplicity and compatibility with silicon technology. A remarkable aspect of this approach is that the SnD_4 precursor not only provides the necessary Sn atoms but also plays a critical role in promoting low-temperature layer-by-layer growth on the Si substrates. In fact, the use of pure digermane under the same conditions does not produce any measurable film growth. It appears that the SnD_4 mediates lateral diffusion and at the same time promotes the rapid evolution of stable H_2 byproducts from the growth front, leaving behind thick and monocrystalline layers with uniform thicknesses and atomically flat surfaces.

For the past few years the CVD growth conditions for films with Sn contents of 2% and higher have been systematically refined,[9,12] with the goal of achieving significant absorption over the entire range of telecommunication windows (a $Ge_{0.98}Sn_{0.02}$ alloy has the same bandgap as an $In_{0.53}Ga_{0.47}As$ alloy lattice-matched to InP, a standard near-infrared detector material) along with eventually demonstrating a direct gap alloy (predicted for Sn concentrations in the 6–11% range[13]). On the other hand, there are applications for which smaller Sn concentrations may be sufficient and even desirable. For example, using the known compositional dependence of the direct bandgap, we estimate that only 0.2% of Sn is needed to double the room-temperature absorption coefficient at 1550 nm relative to pure Ge.[9] Detectors based on such very diluted alloys would have the benefit of increased responsivity while keeping alloy scattering to a minimum. Such small amounts of Sn might also be useful for improving the performance of the recently demonstrated Ge-on-Si laser structures,[14] since the addition of Sn monotonically reduces the separation between the direct and indirect minima in the conduction band of Ge.

In principle, lower Sn concentrations can be achieved in the material by reducing the partial pressure of SnD_4 in the reaction mixture. However, since the presence of SnD_4 also plays a critical role in promoting layer-by-layer growth, the question arises as to what extent is it possible to reduce the Sn concentration without compromising film quality. In this paper, we show that Ge-like materials incorporating very low Sn contents in the 0.15–0.3% Sn range ($\sim$7–13 $\times 10^{19}$ atoms/cm^3) can be formed in a controlled and reproducible manner.

For standard Ge-on-Si material, the low absorption at 1550 nm creates serious difficulties for integrated detectors on Si platforms. In the case of normal-incidence devices, attempts to compensate the poor absorption by utilizing thicker films lead to reduced bandwidth.[15–18] Waveguide geometries make it possible to decouple the bandwidth from responsivity, but even these structures would benefit from increased absorption at 1550 nm. The standard approach to effect this increase is the introduction of tensile strain,[19] which appears in Ge films on Si due to the thermal expansion mismatch between the two materials.[20] However, the magnitude of this strain depends strongly on the growth conditions. In particular, it usually requires high growth temperatures

[a)]Author to whom correspondence should be addressed. Electronic mail: radek.roucka@asu.edu.

 © 2011 American Institute of Physics

which are incompatible with CMOS fabrication. The incorporation of Sn is a simpler approach that does not rely on strain and can be accomplished at extremely low growth temperatures. The addition of 0.20% of Sn lowers the bandgap of Ge by the same amount as a tensile strain of 0.05%. Additional increases in the Sn concentration to the 1–2% range generate diminishing returns, since the absorption edge has the shape of a step function whereas alloy scattering (and the smaller energy of optic phonons in $Ge_{1-y}Sn_y$) will reduce the carrier saturation velocity which determines the detector's cutoff frequency.[15,21] To investigate this delicate balance, we compare the performance of prototype detectors containing either very diluted $Ge_{1-y}Sn_y$ alloys or pure Ge layers. The results confirm that the Sn-doped Ge leads to devices which display a substantial responsivity enhancement at 1550 nm and, at the same time, improved *I-V* characteristics relative to prior $Ge_{1-y}Sn_y$ *pin* diodes.

II. FILM GROWTH

The depositions of the Sn-doped systems are conducted via SnD_4-assisted reactions of pure digermane directly on Si(100) at a low-temperature of $T = 390$ °C and pressure of $P = 0.300$ Torr. The Sn concentration in the films is varied in the 10^{19}–10^{20} cm^{-3} range by increasing the amount of SnD_4 in the reaction mixture while keeping the growth temperature constant. Under these conditions, we find that the growth rate increases significantly in proportion to the amount of SnD_4, reaching a maximum value of ~20 nm/min that facilitates the growth of films with thicknesses exceeding 1 μm. Below the critical concentration of 10^{19} cm^{-3} Sn, the growth rate diminishes to a nearly impractical level, while well above the 10^{20} cm^{-3} level the material produced is more characteristic of the $Ge_{1-y}Sn_y$ alloys previously reported. Using the narrow processing window of temperature, pressure, and Sn concentration just described, thick layers with flat surfaces and minimal dislocation densities are produced, thereby circumventing the Stranski–Krastanov mechanism that characterizes the growth of Ge on Si. It is apparent that the presence of SnD_4 promotes a layer-by-layer crystal assembly while maintaining unprecedented high growth rates at the low temperature employed. Conversely, as stated above, the use of pure digermane under the same conditions does not produce any measurable film growth.

Extensive characterizations of the as-grown layers were performed using Rutherford backscattering (RBS), atomic force microscopy (AFM), Nomarski microscopy, cross-sectional transmission electron microscopy (XTEM) and x-ray diffraction (XRD). The RBS signal under channeling alignment (χ_{min}) for the films shows extremely low values, and the AFM/Nomarski images reveal smooth surfaces entirely devoid of defects and imperfections. The XTEM phase-contrast micrographs confirm the flat surface morphology and indicate that the bulk material is relatively free of threading defects [see Fig. 1(a)]. High-resolution imaging experiments detect the presence of periodic edge-type dislocations confined to the interface plane [Fig. 1(b)], accommodating the significant lattice mismatch between the substrate and the films. The strain state of the film is determined by high resolution XRD measurements of the (224) reciprocal space maps and (004) peaks. Rocking scans of the (004) peaks reveal a FWHM of 800-900 arc sec, which is significantly reduced by rapid thermal annealing processing of the samples using a sequence of three 10 s cycles of heating at 680 °C. The procedure markedly sharpens the XRD peak, leading to a reduction of the FWHM down to 145 arc sec. After annealing, the film surface remains flat (RMS ~ 1 nm) and the layer RBS channeling is dramatically improved with final χ_{min} values in the range of 5–10%, which are close to the experimental limit for bulk Si wafers.

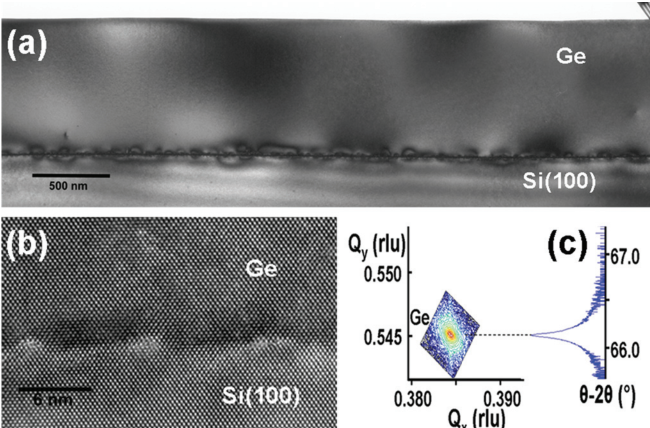

FIG. 1. (Color online) (a) High-resolution electron micrograph of 1 μm thick film containing dopant levels of Sn ($10^{19}/cm^3$). The area within the field of view appears completely devoid of threading defects and exhibits a flat surface. (b) Hig-resolution image showing edge- type dislocations localized to the interface between Ge and Si(100). (c) High-resolution XRD plots indicate a nearly strain-free state and very narrow mosaic spreads as evidenced by sharp and intense (224) reciprocal space maps and (004) peaks. A rocking curve of the latter exhibits a FWHM of 140 arc sec, which is well beyond the state-of-the-art of Ge on Si materials.

Since the Sn content in these samples is near the RBS detection limit, we conducted SIMS elemental analysis of the annealed layers which revealed a highly homogeneous profile of the element throughout the crystal at concentrations of around 10^{19} atoms/cm^3. The SIMS data were calibrated using reference films containing 0% Sn (pure Ge) and 1.5% Sn as measured by RBS. Under the growth conditions employed here the Sn does not function as a surfactant but is incorporated as a fully substitutional atom in the average diamond lattice of the Ge-like material, as expected.

In prior work we showed that there is an inverse relationship between the growth temperature and the level of Sn incorporation into the Ge lattice via this CVD approach. For example, alloys containing 0.6–3.0% Sn are produced at 380–340 °C. The doping levels obtained here follow this trend and produce a true random solid solution with intrinsic structural properties and thermal stability close to those of the parent Ge material.

III. MATERIAL CHARACTERIZATION

A. Electrical properties

Electrical measurements were conducted on a series of films with thicknesses of ~0.5–1 μm with a particular focus on samples with compositions in the 0.06–0.10% Sn range to

Downloaded from http://pubs.aip.org/aip/jap/article-pdf/doi/10.1063/1.3592965/15075199/103115_1_online.pdf

TABLE I. Summary of electrical measurement data (carrier concentration, N; Hall mobility, μ; resistivity, ρ) for a range of samples containing 0.0–0.1% Sn, obtained at room temperature using two contact methods.

Thickness (nm)	% Sn	N (cm^{-3})	μ (cm^2/V.s)	ρ (Ω.cm)	Contact
500	0.00	3.60×10^{16}	8.30×10^2		
800	0.06	2.60×10^{16}	3.88×10^2	0.70	Indium
1100	0.10	2.70×10^{16}	2.74×10^2	0.95	
500	0.00	4.10×10^{16}	7.21×10^2	0.24	
800	0.06	2.85×10^{16}	3.45×10^2	0.72	Cr(20nm)/ Au(200nm)
1100	0.10	1.76×10^{16}	3.57×10^2	1.12	

compare their behavior to that of pure Ge. The Hall mobility, resistivity, and carrier concentrations for representative films and a reference pure Ge counterpart (grown via the gas-source MBE method[22]) are listed in Table I. Pure Ge samples are generally n-type ($\sim 7 \times 10^{15} - 3 \times 10^{16}/cm^3$) as–grown, and for the purpose of comparison we have counter-doped them with diborane at the appropriate levels. Being mindful of the fact that ohmic contacts are difficult to produce on Ge-like materials, we employed two types of metal contacts to establish the reproducibility of the measurements. As seen in Table I, we obtain similar values for the two types of contact. We find that the samples are p-type, with carrier concentrations in the 10^{16} cm^{-3} range. The measured hole mobility for the pure Ge films—$\mu_h = 700$–800 cm^2 V^{-1} s^{-1} is about one-half the mobility $\mu_h = 1500$ cm^2 V^{-1} s^{-1} obtained in bulk Ge samples with similar hole concentrations.[23] We speculate that this reduced mobility is due to carrier scattering at the Si-Ge interface. We observe an additional factor of $\sim$2 reduction in mobility when comparing the Sn-doped samples with pure Ge. At carrier concentrations in the 10^{16} cm^{-3} range, the room temperature mobility of bulk Ge is limited by acoustic phonon and ionized impurity scattering.[23,24] Neither mechanism can lead to a halving of the mobility for Sn concentrations as small as 0.06%. In the case of ionized impurity scattering, the only effect of alloying might be a change in screening, but such an effect should be negligible for small Sn concentrations. Similarly, acoustic phonons depend on the material's density and elastic constants, which will change trivially at low Sn concentrations. The only mechanism that might account for the observed decrease in mobility is alloy scattering. In the case of $Ge_{1-x}Si_x$ alloys, their hole mobility is halved, relative to pure Ge, for $x = 0.05$.[25] If we assume that the mobility limited by alloy scattering is of the form[24]

$$\mu_{alloy} = \frac{Ae^2}{x(1-x)U_{AL}^2}, \quad (1)$$

where A is a constant and U_{AL} is the so-called alloy potential, we obtain $A = 77$ cm^2 V s^{-1} using $U_{AL} = 0.9$ eV (Ref. 25) and applying Mathiessen's rule to fit the mobility of $Ge_{0.95}Si_{0.05}$. If we next assume that Eq. (1) is valid for $Ge_{1-y}Sn_y$ alloys with the same value of A, a similar fit of the experimental mobilities in Table I requires that U_{AL} = 12 eV, about one order of magnitude larger than in $Ge_{1-x}Si_x$ alloys. Such an increase is not unreasonable if we consider the fact that the alloy potential is also responsible for the observed bowing in the compositional dependence of the optical transition energies. In the case of the lowest direct gap E_0, which involves the hole states that contribute to the mobility, the bowing parameter is indeed one order of magnitude larger in $Ge_{1-y}Sn_y$ alloys relative to $Ge_{1-x}Si_x$ alloys.[13] These crude estimates confirm that alloy scattering is a plausible explanation for the observed decrease in mobility in the Sn-doped samples. The reason for the enhanced alloy potential in $Ge_{1-y}Sn_y$ alloys is the much larger size and Phillips electronegativity mismatch between Ge and Sn as compared to the mismatch between Si and Ge.[13]

B. Device studies

A *pin* photodiode [Fig. 2(a)] was fabricated on a a highly doped n-type Si(100) wafer (bottom electrode) with a resistivity of $\rho = 0.003$ Ω cm. The diode consists of a $\sim$450 nm thick nominally intrinsic $Ge_{0.9975}Sn_{0.0025}$ ($\sim 1.1 \times 10^{20}$ cm^{-3} Sn) film followed by a 150 nm p-type $Ge_{0.9997}Sn_{0.0003}$ capping layer ($\sim 1.0 \times 10^{19}$ cm^{-3} Sn). The purpose of the lower Sn content in the top layer was to minimize the 1550 nm absorption above the intrinsic region of the diode. The layers were grown using digermane and stannane, as previously described. For the p-type layer, appropriate amounts of diborane were included in the reaction mixture. After growth, the samples were subjected to three cycles of rapid thermal annealing at 680 °C for 10 s each. The RBS analysis indicates a nominal thickness of 590 nm for the entire film, and an average Sn content near the detection limit. The channeled spectrum shows a high degree of epitaxial alignment and excellent crystalline quality, as expected. The SIMS elemental profiles indicate a uniform

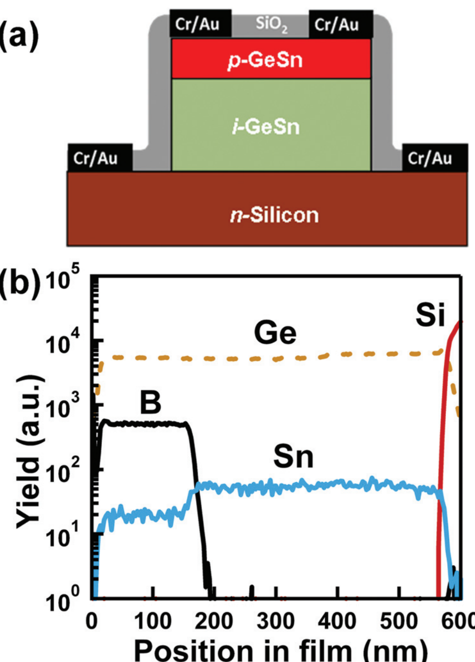

FIG. 2. (Color online) (a) Schematic representation of the Ge-based photodiode in n-Si(100)/i-GeSn/p-GeSn geometry. (b) Corresponding SIMS elemental profiles showing the distribution of B, Sn, Ge, and Si atoms throughout the entire film structure.

Downloaded from http://pubs.aip.org/aip/jap/article-pdf/doi/10.1063/1.3592965/15075199/103115_1_online.pdf

distribution of the Sn substituents and the B dopants, as shown in Fig. 2(b). Note that both the Sn and B profiles show a steep and abrupt step at the interface between the *p*-doped and intrinsic region, indicating minimal interdiffusion. A calibration of the mass yield gives the Sn concentrations quoted in the preceding text. Both the on-axis XRD plots and the (224) reciprocal space maps reveal a single peak corresponding to a tetragonally distorted diamond-structure lattice with the dimensions $a = 5.6658$ Å and $c = 5.6553$ Å. Using elastic constants for Ge, (Ref. 26), we obtain a relaxed lattice parameter, $a_0 = 5.6598$ Å. If we use the lattice parameter (in Å) $a_0(y) = 5.6575(1-y) + 6.4894y + 0.063y(1-y)$ for relaxed $Ge_{1-y}Sn_y$ alloys, where the bowing parameter was obtained from Chizmeshya's *et al. ab initio* calculations,[27] we obtain $y = 0.26\%$ from the *x*-ray data, which is in very good agreement with the SIMS calibration for the intrinsic layer. Our inability to resolve the two layers is probably due to their close similarity and the much larger thickness of the intrinsic layer.

The samples were processed using protocols similar to those employed to fabricate pure Ge and $Ge_{0.98}Sn_{0.02}$ photodiodes, as previously described.[28] In this case, circular mesas with diameters ranging from 50 μm to 3 mm were defined by photolithography and etched by using reactive ion plasmas generated by gaseous BCl_3. The mesas were passivated by a 270 nm thick SiO_2 layer which also serves as an antireflection coating. The Cr/Au metal contacts were deposited by e-beam and defined by lithography.

Current-density versus voltage measurements were conducted and a representative curve for a typical 100 μm device is shown in Fig. 3(a), where it is compared with data measured from a similar pure-Ge-on-Si device consisting of a 390 nm intrinsic layer, a 100 nm *p*-type top layer, and a 420 nm SiO_2 cap layer. The curves exhibit a similar rectifying behavior, but with a somewhat better ideality factor (1.2) in the Ge device than in the $Ge_{0.9975}Sn_{0.0025}$ device (1.3). The dark current densities at -1 V are about one order of magnitude higher in the $Ge_{0.9975}Sn_{0.0025}$ device. On the other hand, similar diodes based on $Ge_{0.98}Sn_{0.02}$ layers show dark currents close to 10 A cm^{-2}, so that the Sn-doped material represents a significant improvement over *bona fide* alloys. In the case of the pure Ge device, the dark current has a thermal activation energy $E_a = 0.32$ eV at $V = -1$ V, which is close to to $E_g/2$, where E_g is the fundamental bandgap.[28] This clearly indicates a Shockley-Read-Hall (SRH) generation mechanism. In the Sn-doped material, substitutional Sn has a measurable impact on carrier mobilities via alloy scattering, but it can be ruled out as the source of additional SRH trap states due to the isoelectronic nature of Sn and Ge. In fact, a study of the temperature dependence of the dark current [Fig. 3(b)] reveals an activation energy of $E_a = 0.17$ eV at -1 V, which is substantially below the value of E_a obtained in the pure Ge diode. This indicates that the excess dark current in the Sn-doped device is not due to enhanced SRH generation but to some alternative mechanism.

Very low values of the activation energy have been associated with tunneling transitions.[29,30] At this point, it is unclear if the defects that cause the excess dark current in the Sn-doped diodes are located at the interface with the Si substrate or in the material's bulk. The microstructural similarities between the pure-Ge-on-Si and Sn-doped Ge-on-Si interfaces, combined with the observation of a standard SRH mechanism in the pure-Ge-on-Si diodes, suggest a bulk origin for the excess dark current in the Sn-doped devices. However, the detailed mechanism by which layer-by-layer growth proceeds at the interface with Si may be very different in the two cases, since the pure-Ge material is grown by gas-source molecular beam epitaxy of Ge_2H_6 assisted by the $CH_2(GeH_3)_2$ metal-organic additive,[22] whereas the Sn-doped material is grown via CVD of Ge_2H_6 in the presence of SnD_4. Thus, one cannot rule out the possibility that different types of interface states may be generated by each of these growth processes. Further investigations of this issue will require systematic studies of devices with varying Sn concentrations and thicknesses. It is interesting to note that in diodes based on $Ge_{0.98}Sn_{0.02}$ layers the measured dark count activation energy at -1 V is even smaller ($E_a = 0.09$ eV; Ref. 28) Thus, the intermediate E_a value obtained for the $Ge_{0.9975}Sn_{0.0025}$ device may signal the onset of a transition from tunneling to SRH generation. A final point to consider regarding the *I-V* characteristics is that our investigations of the dependence of the dark current density on the device diameter suggests that the leakage currents do not originate from the sidewalls of the mesas.

The spectral responsivity at zero bias for the two diodes in Fig. 3 is shown in Fig. 4. The measurements were performed by focusing the monochromatized light from a halogen lamp

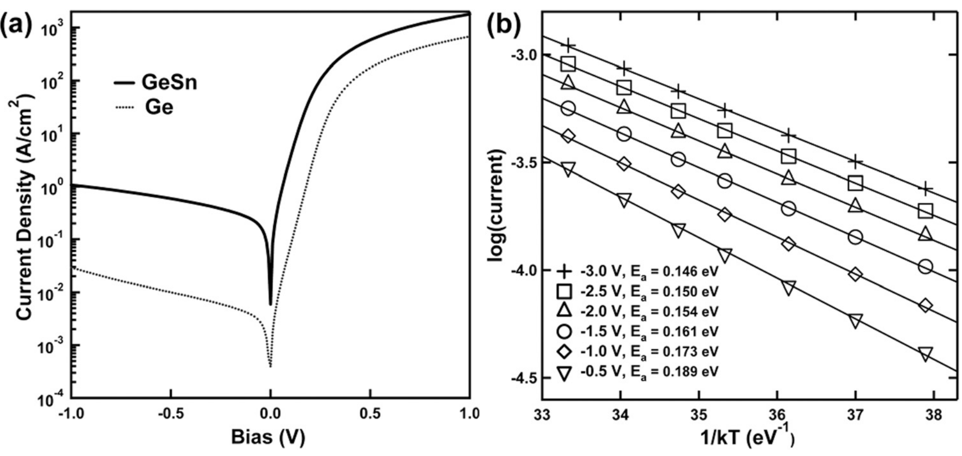

FIG. 3. (a) *I-V* graphs obtained from the GeSn sample and Ge reference device mesas with sizes of 100 μm in diameter. (b) Arrhenius plots of the dark current density at selected reverse bias values. Activation energies are obtained from the line slopes.

Downloaded from http://pubs.aip.org/aip/jap/article-pdf/doi/10.1063/1.3592965/15075199/103115_1_online.pdf

onto the surface of the devices using optical fibers. The light was modulated with a mechanical chopper. The diode photocurrent induced a voltage on a 10 kΩ load resistor that was measured with a lock-in amplifier. The incident power was obtained by measuring the light passing through an aperture with a diameter identical to that of the device. The absolute responsivities are not directly comparable because the layer thicknesses are not identical, but the optical properties of the component materials manifest themselves in the different spectral dependences of the responsivity. The large drop in responsivity beyond ∼1600 nm is associated with the lowest direct bandgap of these materials near 0.8 eV. Superimposed with the steplike onset of the responsivity at 1600 nm we see oscillations at shorter wavelengths that are due to interference effects. These are enhanced by computing the derivatives $dR/d\lambda$ of the responsivities, as shown in Fig. 5.

The most striking feature in Figs. 4 and 5 is the clear shift to longer wavelengths in the responsivity onset corresponding to the Sn-doped device, indicating a direct bandgap reduction that is clearly measurable even for a Sn concentration as low as 0.25%. We also note that this shift is not accompanied by a broadening of the absorption edge, as seen in the case of $Ge_{0.98}Sn_{0.02}$ alloys, for which a Gaussian broadening as high as 70 meV was needed to fit the experimental absorption.[28] Indeed, the direct gap onset appears to be slightly sharper in the Sn-doped device. Since the observed shift between the two diodes is comparable in magnitude to those typically induced by strain, a detailed model is needed to quantify the relative contributions from composition and strain. The model must also account for the interference effects caused by the optical mismatch of the different layers. In Ref. 28 we modeled the device responsivity as

$$R = \left(\frac{e\lambda}{hc}\right)\left[f\eta_c(1 - T_+ - R_+) + \exp(\alpha_{top}d_{top})f\eta_c T_+ R_{back}(1 - T_- - R_-)\right]. \quad (2)$$

Here, e is the electron charge, λ is the wavelength, h is Planck's constant, c is the speed of light, η_c is the collection efficiency, T_+ (R_+) is the transmittance (reflectance) of the entire oxide/diode stack on Si under illumination from the top surface, R_{back} is the reflectance at the back surface of the Si wafer, T_- (R_-) is the transmittance (reflectance) of the oxide/diode stack for illumination by the light reflected from the back surface, α_{top} the absorption coefficient of the top p-type layer, and d_{top} its thickness. The factor

$$f = \frac{1 - \exp(-\alpha_{int}d_{int})}{\exp(\alpha_{top}d_{top}) - \exp(-\alpha_{int}d_{int})}, \quad (3)$$

where α_{int} is the absorption coefficient and d_{int} is the thickness of the intrinsic layer, yields the fraction of the incoming

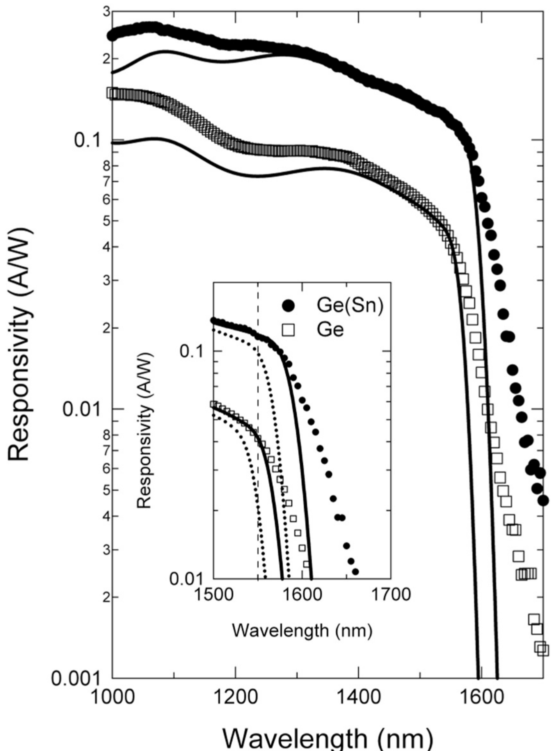

FIG. 4. Responsivities of heterostructure *pin* diodes on n-type Si substrates. Solid circles correspond to a device with a $Ge_{0.9975}Sn_{0.0025}$ intrinsic layer (490 nm); empty squares correspond to a device with a pure Ge intrinsic layer (350 nm). The solid lines represent a fit with the theoretical model described in the text, using the independently measured composition and strain values. The inset shows the region near 1550 nm in more detail. The dotted lines show the expected responsivity if the layers were perfectly strain-free. The vertical dashed line marks the 1550 nm wavelength.

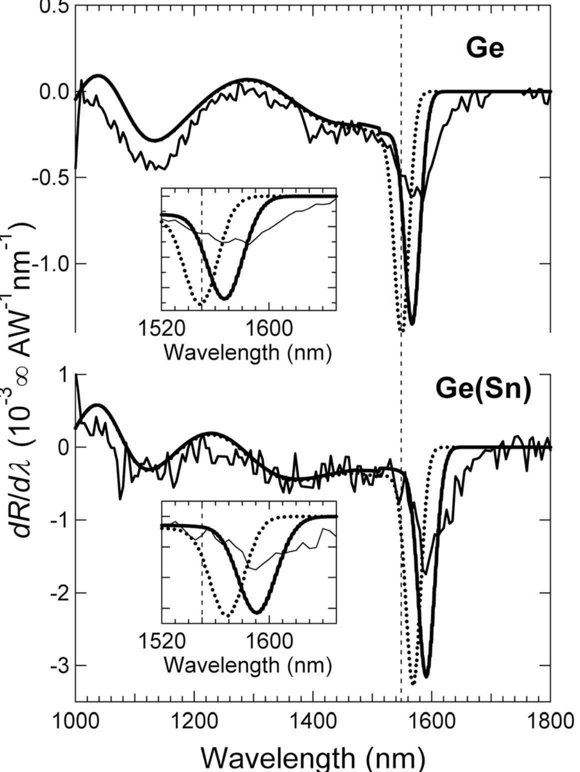

FIG. 5. Responsivity derivatives for the two diodes in Fig. 4. The thin solid lines are numerical derivatives of the experimental data. The thick solid lines correspond to the derivatives of the model responsivities in Fig. 4, and the dotted lines are the derivatives of the same theoretical calculations but setting the strain equal to zero. The vertical line corresponds to 1550 nm. The insets show the spectral region around this wavelength in more detail.

Downloaded from http://pubs.aip.org/aip/jap/article-pdf/doi/10.1063/1.3592965/15075199/103115_1_online.pdf

light absorbed in the intrinsic layer of the structure, which is assumed to provide the only contribution to the photocurrent. The corresponding fraction for the light reflected at the back surface is $f\exp(\alpha_{top}d_{top})$. Equation (3) treats the light traveling through the device structure as fully coherent, but neglects the coherency between the light traveling toward the back surface of the Si wafer and the light reflected at this surface. This should be an excellent approximation given the macroscopic thickness of the Si wafer.

The transmittances and reflectances needed for Eq. (3) are calculated using standard transfer-matrix techniques. For this purpose, in Ref. 28 we used tabulated optical constants for SiO_2, Ge, $Ge_{0.98}Sn_{0.02}$, and Si, but this approach is clearly impractical if we want to explore the effects of strain and composition. The alternative for the active layers of our devices is to use the analytical model introduced in Ref. 9. The model provides a remarkably accurate account of the direct gap absorption in pure Ge based on elementary $\boldsymbol{k}\cdot\boldsymbol{p}$ theory, and therefore, it can be used for $Ge_{1-y}Sn_y$ alloys by inserting the experimental compositional dependence of the relevant optical transitions. Moreover, since the model accounts for the absolute value of the absorption without any adjustable parameter, it can be used to predict not only shifts in the absorption edge but also the compositional dependence of the absorption strength, which is particularly important for modeling responsivities. Strain effects can also be easily included via deformation potential theory. A disadvantage of the model, however, is that it is limited to the spectral region immediately around the material's direct gap. Since the experimental responsivity in Fig. 4 covers a wider range down to 1000 nm, we have simply added a corrective term to fit the experimental absorption up to this wavelength. The resulting hybrid approach, in which the E_0 absorption is computed from "first principles" while the above-E_0 absorption is empirically fit to the experimental data, provides a convenient tool for studying subtle changes around E_0 while yielding quantitative responsivity estimates over a much wider range. The details of this hybrid absorption model are provided in the Appendix.

The calculated responsivities for the two devices are shown in Fig. 4 and their derivatives appear in Fig. 5. For these calculations, we use the measured strains of 0.11% in the intrinsic layer of the Sn-doped device and 0.088% in the pure-Ge device. The bandgap of the $Ge_{1-y}Sn_y$ alloy was interpolated between that of Ge and α-Sn using the standard expression, $E_0(y) = E_0^{Ge}(1-y) + E_0^{Ge} - by(1-y)$ with $E_0^{Ge} = 0.803$ eV, $E_0^{Sn} = -0.4$ eV, and $b = -2.5$ eV (Ref. 31). The overall thickness of the intrinsic and p-doped layer was adjusted to match the oscillations in Fig. 5, and the result was within 5% of the value determined from the RBS measurements. The collection efficiency was fit to the experimental responsivity at 1550 nm, and we obtained $\eta_c = 0.67$ for the Sn-doped diode and $\eta_c = 0.38$ for the pure-Ge diode. These less- than-perfect collection efficiencies at zero bias are probably related to the 10^{16} cm^{-3} residual doping in the intrinsic layers. It is apparent from Fig. 4 that the collection efficiencies are higher at short wavelengths.

At long wavelengths, the drop in the theoretical responsivity curve is much sharper than experimentally observed, an effect that can also be seen in the derivative profiles. This is because our simulation does not include indirect gap absorption. In spite of this limitation, the model accounts very well for the relative spectral shift between the two diodes. To understand the contributions to this shift, we show in the inset to Figs. 4 and 5 (as dotted lines) the expected responsivities and their derivatives in the absence of any strain. The effect of strain and composition are seen to be of the same order of magnitude.

The derivative curves in Fig. 5 offer an easy graphical interpretation of the "diminishing returns" condition mentioned in the Introduction. The negative peak near 1550 nm represents the spectral range over which the responsivity changes rapidly as a function of strain and/or composition. Once this peak is to the right (longer wavelengths) of the vertical line corresponding to 1550 nm, further increases in Sn concentration and/or tensile strain lead to much smaller gains in responsivity. It is apparent that our Sn-doped sample has a nearly ideal combination of tensile strain and composition to meet this condition. To accomplish the same result based solely on pure Ge, a tensile strain level of 0.2% would be needed. In fact, such a detector was fabricated by Liu *et al*. (Ref. 19). They report a responsivity of $R = 0.56$ A/W at 1550 nm from a 2410 nm-thick Ge-on-Si diode in which a tensile-strain level of 0.2% is obtained by growing the bulk of the Ge layer at 700 °C and annealing the sample at 900 °C. At 1550 nm and assuming $\eta_c = 1$, our model predicts a responsivity of $R = 0.55$ A/W for this diode—in very good agreement with the experimental value—and $R = 0.54$ A/W

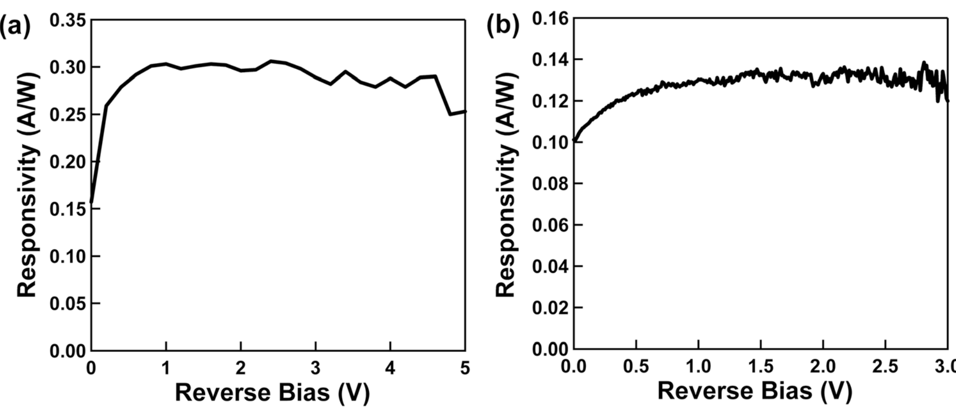

FIG. 6. Responsivity vs bias under illumination by a laser diode at (a) 1300 nm and (b) 1550 nm.

Downloaded from http://pubs.aip.org/aip/jap/article-pdf/doi/10.1063/1.3592965/15075199/103115_1_online.pdf

from a detector based on a material with the same Sn concentration and strain level as in our Sn-doped Ge. On the contrary, if we want to obtain the same responsivity using perfectly relaxed Sn-doped layers, we need a Sn concentration of 0.6%. This is less than the concentration of 0.8% that would be needed to match the lowest direct bandgap in both materials, following the analysis in the Introduction. The discrepancy can be understood by recalling that strain broadens the absorption edge due to the light-heavy hole splitting. While this broadening is very small in the derivative profiles shown in Fig. 5, a similar plot for a tensile strain level of 0.2% shows clear evidence of the separate absorption edges associated with the light- and heavy-hole bands.

For $\eta_c = 1$, our model predicts $R = 0.30$ A/W at 1300 nm and $R = 0.17$ A/W at 1550 nm for our Sn-doped sample. In Fig. 6 we show the bias dependence of the responsivity at these two wavelengths and we see that at 1300 nm we do approach complete carrier collection at reverse biases above 0.5 V. Conversely, at 1550 nm the asymptotic value of the responsivity is 0.13 A/W, which corresponds to a collection efficiency of $\eta_c = 0.74$. These bias-dependence measurements were carried out under laser illumination, and therefore the zero bias values are probably not directly comparable to those obtained under much weaker lamp illumination.

IV. CONCLUSIONS

In conclusion, we have shown that doping-level amounts of Sn are sufficient to engineer the optical properties of Ge around the critical 1550 nm wavelength. The manipulation of the absorption edge via Sn doping makes it possible to decouple the conditions that produce the highest-quality growth (which normally determine the final strain level in the material) from the desired value of the absorption edge, which is controlled by both strain and composition. Using the Sn concentration as an adjustable parameter, large increases in responsivity can be achieved while keeping the growth temperature at very low values compatible with CMOS processing. The same increases in responsivity using pure Ge layers require high levels of tensile strain that can only be achieved at much higher processing temperatures. Compared with previously published results using $Ge_{0.98}Sn_{0.02}$ alloys, the much lower Sn concentrations in the Sn-doped samples virtually eliminate alloy broadening of the optical transitions, and lead to dark current densities that are one order of magnitude lower. The results suggest that Sn-doped Ge has an intriguing potential in the field of silicon photonics.

ACKNOWLEDGMENTS

We would like to thank Dr. John Tolle for electron microscopy imaging. This work was supported by the U.S. Air Force under DOD AFOSR Contract No. FA9550-06-01-0442 (MURI program), by the Department of Energy under Contract No. DE-FG36-08GO18003, and by the National Science Foundation under Grant No. DMR-0907600. Y. K. Yeo would like to acknowledge AFOSR/NE support through Grant No. F1ATA00083G003 (Gernot Pomrenke).

APPENDIX

We express the absorption in Ge-like materials as

$$\alpha(E) = \alpha^{E_0}(E) + \alpha^{\text{high}}(E). \tag{A1}$$

The first term accounts for the absorption related to the lowest direct bandgap, E_0, and the second term incorporates above-bandgap transitions. Indirect transitions below the direct gap are not included. The E_0 transitions involve the heavy- and light-hole valence bands and the *s*-like conduction band near the $\boldsymbol{k} = 0$ (Γ) point in the Brillouin zone. The dispersion of all of these bands is assumed to be parabolic. We express the E_0 absorption as

$$\alpha^{E_0}(E) = \alpha_0^{chh}(E)[f_{hh}(E) - f_c(E)] + \alpha_0^{clh}(E)[f_{lh}(E) - f_c(E)]. \tag{A2}$$

Here, the superscripts *chh* (*clh*) refer to transitions between the heavy-hole band *hh* (light-hole band *lh*) and the conduction band, *c*. The quantity, $\alpha_0^{cv}(E)$, with $v = hh$ or lh is the absorption coefficient for an empty conduction band and a full valence band. The Fermi functions, $f_v(E)$ and $f_c(E)$, give the occupation probability for the valence and conduction band states separated by an energy E. We express the absorption in terms of the real (ε_1) and imaginary (ε_2) parts of the empty-band dielectric function as $\alpha_0^{cv}(E) = E\varepsilon_2^{cv}(E)/[\hbar c\sqrt{\varepsilon_1(E)}]$, where c is the speed of light and $\hbar = h/(2\pi)$. Since the value of ε_1 changes very little at the E_0 gap, for the real part we simply use an expression of the form, $\varepsilon_1(E) = 11.03 - 11.88/(E - 2.62)$, with E in eV, which has been fit to the experimental real part of the dielectric function in pure Ge. The compositional and strain dependence of ε_1 are neglected. For each of the $v = hh$ heavy- and $v = lh$ light-hole components, the imaginary part of the dielectric function is written as,

$$\varepsilon_2^{cv}(E) = \varepsilon_x^{cv}(E) + \varepsilon_f^{cv}(E)S^{cv}(E), \tag{A3}$$

where ε_x^{cv} the below-bandgap excitonic contribution given by,[32]

$$\varepsilon_2^{cv}(E) = \frac{16\pi|P|^2e^4\mu_{cv}^2R_{cv}}{E^2\hbar^2m^2\varepsilon_0}\sum_{n=1}^{\infty}\frac{1}{n^3}\delta(E - E_n), \tag{A4}$$

where P is the momentum matrix element, e and m are the free electron charge and mass, respectively, μ_{cv} is the reduced electron-hole mass, ε_0 is the static dielectric constant, and the Rydberg constant is defined as $R_{cv} = \mu_{cv}e^4/(2\hbar^2\varepsilon_0^2)$. With this definition, the excitonic energy levels can be written as $E_n = E_{0v} - R_{cv}/n^2$, where E_{0v} is the light-hole (heavy-hole) direct bandgap for $v = lh$ ($v = hh$). The second term in Eq. (A3) is given by the dielectric function, ε_f^{cv}, for free, uncorrelated electron-hole pairs multiplied by the Sommerfeld enhancement factor, S^{cv}. These quantities are given by,[32]

$$\varepsilon_f(E) = \frac{4\sqrt{2}e^2P^2\mu_{cv}^{3/2}}{3m^2\hbar E^2}(E - E_{0v})^{1/2}\Theta(E - E_{0v}), \tag{A5}$$

and

$$S^{cv}(E) = \frac{\tau_{cv}e^{\tau_{cv}}}{\sinh\tau_{cv}}; \quad \tau_{cv} = \pi\left|\frac{R_{cv}}{E - E_{0v}}\right|^{1/2}. \tag{A6}$$

Downloaded from http://pubs.aip.org/aip/jap/article-pdf/doi/10.1063/1.3592965/15075199/103115_1_online.pdf

Here, $\Theta(x)$ is the unit step function.

The needed $E_{0v} = E_{0lh}$ light-hole direct gap and and $E_{0v} = E_{0hh}$ heavy-hole direct bandgap are calculated as a function of the strain using standard deformation potential theory. The corresponding expressions are,

$$E_{0lh} = E_0 + \frac{\Delta_0}{2} + \delta E_0 - \frac{1}{4}\delta E_{001} - \frac{1}{2}\sqrt{\frac{9}{4}(\delta E_{001})^2 + \Delta_0^2 + \Delta_0 \delta E_{001}},$$
$$E_{0hh} = E_0 + \delta E_0 + \frac{1}{2}\delta E_{001}. \tag{A7}$$

Here, Δ_0 is the spin-orbit splitting at the Γ-point of the Brillouin zone and

$$\delta E_0 = 2a_h(1 - C_{12}/C_{11})\varepsilon_{\parallel},$$
$$\delta E_{001} = -2b(2C_{12}/C_{11} - 1)\varepsilon_{\parallel}, \tag{A8}$$

where $\varepsilon_{\parallel} = (a - a_0)/a_0$, C_{11} and C_{12} are elastic constants, a_h is the hydrostatic E_0 gap deformation potential, and b is the shear deformation potential.

For pure Ge, all parameters needed for the evaluation of Eqs. (A3)–(A8) are independently measured (including the matrix element, P, which is obtained from the experimental effective masses using $\boldsymbol{k}\cdot\boldsymbol{p}$ theory), and the values we use are summarized in Table II. For $Ge_{1-y}Sn_y$ alloys the band structure parameters are interpolated in the spirit of $\boldsymbol{k}\cdot\boldsymbol{p}$ theory as discussed in Ref. 9. The deformation potentials and elastic constant ratio, C_{12}/C_{11}, are linearly interpolated with those of α-Sn. Of course, given the doping-level amounts of Sn in this work, the interpolated values are virtually identical to those of pure Ge. The only compositional dependence that plays a critical role in our simulations is that of the direct gap E_0, which, as indicated above, is taken as $E_0(y) = E_0^{Ge}(1-y) + E_0^{Ge} - by(1-y)$ with $E_0^{Ge} = 0.803$ eV, $E_0^{Sn} = -0.4$ eV, and $b = -2.5$ eV (Ref. 31).

The occupation probability functions f_c, f_{lh}, and f_{hh} depend on the Fermi level, E_F. The effect of doping on the absorption coefficient is partially included by computing the value of E_F corresponding to the layer's doping concentration. In the case of the nominally intrinsic layer, $f_c = 0$ and $f_{lh} = f_{hh} = 1$ is an excellent approximation. For $p > 10^{19}$ cm^{-3} the effect of doping on the absorption is not negligible, but it has a small effect on our computed responsivities because the top p-layer is thin and is not assumed to contribute to the photocurrent.

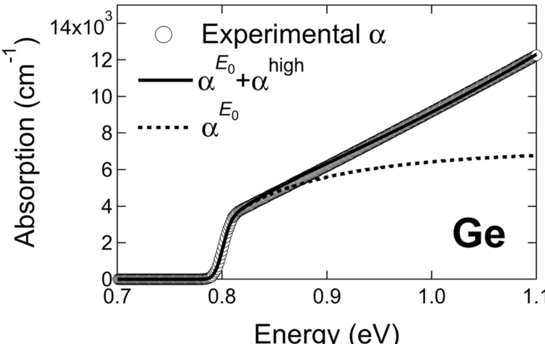

FIG. 7. Experimental optical absorption for Ge (circles). The solid line is the absorption calculated with the model described in the text. The dashed line is the absorption corresponding to the bands that determine the E_0 gap at the center of the Brillouin zone, which is assumed to be parabolic.

TABLE II. Band structure and elastic parameters for pure Ge used to compute the optical absorption. A discussion on the selection of these parameters is given in Refs. 9 and 11.

E_0 (eV)	P^2/m (eV)	μ_{clh}/m	$\mu_{c\eta h}/m$	ε_0	Δ_0 (eV)	a_h (eV)	b (eV)	C_{12}/C_{11}
0.803	12.61	0.0183	0.0300	16.2	0.297	−9.64	−1.88	0.3755

In Fig. 7 we show the experimental absorption in pure Ge and, as a dashed line, the results from Eq. (A2) convolved with a Gaussian with a FWHM of 15 meV. If we attribute this broadening to lifetime effects, a convolution with a Lorentzian appears to be physically more meaningful, and this is what we used in Ref. 9. However, the Gaussian function gives a nearly perfect agreement with the experimental absorption, and therefore we use this approach for our responsivity simulations.

As indicated in Ref. 9, it is critical to include excitonic effects if good agreement with the experiment is desired. It is important to point out that in our calculation this is done by computing the excitonic enhancement separately for the $hh \to c$ and $lh \to c$ transitions. This is clearly not exact, however, the details of the excitonic interaction may not matter in our case because our room temperature broadening is much larger than the exciton binding energy.

Above the bandgap, our calculated absorption falls below the measured one because the electronic bands are not parabolic over a large wave vector range and due to the fact that additional bands contribute to the absorption. We find that for $E < 1.3$ eV, the difference between the experimental and the E_0 absorption is very well described by an empirical expression of the form

$$\alpha^{high}(E) = A\left\{1 - \exp\left[-\frac{\ln(E/E_0)}{B}\right]^2\right\}, \tag{A9}$$

with $A = 1.088 \times 10^5$ cm^{-1} and $B = 1.377$. Since this expression vanishes for $E = E_0$, the contribution of this term to the critical near-bandgap region is negligible. However, it is important to take it into account to be able to model the responsivity over the entire spectral range covered in Fig. 4. In Fig. 7 we show (as a solid line) the absorption using Eq. (A1) and we see that the agreement with the experiment is very good.

[1] S. I. Shah, J. E. Greene, L. L. Abels, Q. Yao, and P. M. Raccah, J. Cryst. Growth **83**, 3 (1987).
[2] O. Gurdal, M.-A. Hasan, Jr., M. R. Sardela, J. E. Greene, H. H. Radamson, J. E. Sundgren, and G. V. Hansson, Appl. Phys. Lett. **67**(7), 956 (1995).
[3] G. He and H. A. Atwater, Appl. Phys. Lett. **68**(5), 664 (1996).
[4] A. S. Saidov, A. S. Razzakov, and E. A. Koshchanov, Tech. Phys. Lett. **27**, 698 (2001).
[5] A. S. Razzakov, Dokl. Phys. **46**, 548 (2001).
[6] J. Taraci, J. Tolle, M. R. McCartney, J. Menendez, M. A. Santana, D. J. Smith, and J. Kouvetakis, Appl. Phys. Lett. **78**, 3607 (2001).
[7] H. Pérez Ladrón de Guevara, A. G. Rodríguez, H. Navarro-Contreras, and M. A. Vidal, Appl. Phys. Lett. **83**(24), 4942 (2003).
[8] H. Pérez Ladrón de Guevara, A. G. Rodriguez, H. Navarro-Contreras, and M. A. Vidal, Appl. Phys. Lett. **84**(22), 4532 (2004).

Downloaded from http://pubs.aip.org/aip/jap/article-pdf/doi/10.1063/1.3592965/15075199/103115_1_online.pdf

[9]Vijay R. D'Costa, Y. Y. Fang, J. Mathews, R. Roucka, J. Tolle, J. Menendez, and J. Kouvetakis, Semicond. Sci. Technol. **24**(11), 115006 (2009).
[10]M. Bauer, J. Taraci, J. Tolle, A. V. G. Chizmeshya, S. Zollner, D. J. Smith, J. Menendez, C. Hu, and J. Kouvetakis, Appl. Phys. Lett. **81**, 2992 (2002).
[11]V. R. D'Costa, Y. Y. Fang, J. Tolle, J. Kouvetakis, and J. Menéndez, Thin Solid Films **518**(9), 2531 (2010).
[12]J. Kouvetakis, J. Mathews, R. Roucka, A. V. G. Chizmeshya, J. Tolle, and J. Menendez, IEEE Photonics J. **2**(6), 924 (2010).
[13]V. R. D'Costa, C. S. Cook, A. G. Birdwell, C. L. Littler, M. Canonico, S. Zollner, J. Kouvetakis, and J. Menendez, Phys. Rev. B **73**(12), 125207 (2006).
[14]J. Liu, X. Sun, R. Camacho-Aguilera, L. C. Kimerling, and J. Michel, Opt. Lett. **35**(5), 679 (2010).
[15]L. Colace, G. Assanto, D. Fulgoni, and N. Lee, J. Lightwave Technol. **26**(16), 2954 (2008).
[16]L. Colace and G. Assanto, IEEE Photonics J. **1**(2), 69 (2009).
[17]M. Morse, T. Yin, Y. Kang, O. Dosunmu, H. D. Liu, M. Paniccia, G. Sarid, E. Ginsburg, R. Cohen, Y. Saado, R. Shnaiderman, and M. Zadka, presented at the 2009 Conference on Optical Fiber Communication—OFC 2009, Piscataway, NJ, 22–26 March 2009 (unpublished).
[18]J. Michel, J. Liu, and L. C. Kimerling, Nat. Photonics **4**(8), 527 (2010).
[19]J. Liu, J. Michel, W. Giziewicz, D. Pan, K. Wada, D. D. Cannon, S. Jongthammanurak, D. T. Danielson, L. C. Kimerling, J. Chen, F. O. Ilday, Franz X. Kartner, and J. Yasaitis, Appl. Phys. Lett. **87**(10), 103501 (2005).
[20]Y. Ishikawa, K. Wada, D. D. Cannon, J. Liu, H.-C. Luan, and L. C. Kimerling, Appl. Phys. Lett. **82**(13), 2044 (2003).
[21]F. M. Bufler, P. Graf, B. Meinerzhagen, B. Adeline, M. M. Rieger, H. Kibbel, and G. Fischer, IEEE Electron Device Lett. **18**(6), 264 (1997).
[22]M. A. Wistey, Y. Y. Fang, J. Tolle, A. V. G. Chizmeshya, and J. Kouvetakis, Appl. Phys. Lett. **90**(8), 082108 (2007).
[23]O. A. Golikova, B. Y. Moizhes, and L. S. Stil'bans, Fiz. Tverd. Tela (Leningrad) **3**(10), 3105 (1961).
[24]M. J. Kearney and A. I. Horrell, Semicond. Sci. Technol. **13**(2), 174 (1998).
[25]M. V. Fischetti and S. E. Laux, J. Appl. Phys. **80**(4), 2234 (1996).
[26]H. J. McSkimin, J. Appl. Phys. **24**(8), 988 (1953).
[27]A. V. G. Chizmeshya, M. R. Bauer, and J. Kouvetakis, Chem. Mater. **15**(13), 2511 (2003).
[28]R. Roucka, J. Mathews, C. Weng, R. Beeler, J. Tolle, J. Menendez, and J. Kouvetakis, IEEE J. Quant. Electron. **47**(2), 213 (2011).
[29]Z. Huang, J. Oh, S. K. Banerjee, and J. C. Campbell, IEEE J. Quantum Electron. **43**(3), 238 (2007).
[30]W. K. Loke, S. F. Yoon, S. Wicaksono, K. H. Tan, and K. L. Lew, J. Appl. Phys. **102**(5), 054501 (2007).
[31]J. Mathews, R. T. Beeler, J. Tolle, C. Xu, R. Roucka, J. Kouvetakis, and J. Menéndez, Appl. Phys. Lett. **97**(22), 221912 (2010).
[32]P. Y. Yu and M. Cardona, *Fundamentals of Semiconductors: Physics and Materials Properties* (Springer-Verlag, Berlin, 1996).

Downloaded from http://pubs.aip.org/aip/jap/article-pdf/doi/10.1063/1.3592965/15075199/103115_1_online.pdf